Asian Journal of Chemistry; Vol. 33, No. 3 (2021), 611-616

ASIAN JOURNAL OF CHEMISTRY

https://doi.org/10.14233/ajchem.2021.22961

Synthesis, Crystal Structure and DFT Studies of 4-(2-(4,5-Dimethyl-2-(3,4,5-trimethoxyphenyl)-1*H*-imidazol-1-yl)ethyl)morpholine

A. Prabhakaran[1], M. Arockia Doss[2,*], E. Dhineshkumar[3] and R. Rajkumar[4,*]

[1]Department of Chemistry, CK College of Engineering and Technology, Cuddalore-607003, India
[2]Department of Chemistry, St. Joseph University, Nagaland-797115, India
[3]Department of Chemistry, Annamalai University, Annamalainagar-608002, India
[4]Department of Chemistry, Thiruvalluvar University College of Arts and Science, Kallakurichi-606213, India

*Corresponding author: E-mail: rajkumarphd.r@gmail.com

Received: 20 August 2020; *Accepted*: 14 January 2021; *Published online*: 16 February 2021; AJC-20257

The title compound 4-(2-(4,5-dimethyl-2-(3,4,5-trimethoxyphenyl)-1*H*-imidazol-1-yl)morpholine (DMTPM) was synthesized using a one-pot multicomponent approach. The molecular structure of the compound was charcterized with ^{1}H & ^{13}C NMR, HR-MS and single-crystal X-ray diffraction. In the ground-state, DMTPM molecular geometry was determined using the DFT based on B3LYP/6-31G(d,p) and compared to the experimental results. In addition, molecular electrostatic potential (MEP) map and molecular frontier orbitals (MFO) were performed and the results obtained were compatible with the electronic properties.

Keywords: 1,2,4,5-Tetrasubstituted imidazole, Multi-component reaction, DFT.

INTRODUCTION

Heterocyclic compounds are the largest and most assorted group of organic compounds. Various heterocyclic compounds are known today and the number is expanding quickly step by step due to its tremendous synthetic approach and their applications in various fields. Nitrogen based heterocycles are of specific significance in the pharmaceutical industries. Among nitrogen based heterocyles, imidazole and its derivatives have recently been reported to draw attention due to their unusual optical properties [1-3]. In preparation for functionalized materials [4-8], these compounds play an exceptionally vital role in chemistry as synthetic reactions for mediators.

Imidazole nucleus also features human species including histidine, vitamin B12 and the component's base DNA structure, purines, histamine and biotin. They also exist in the composition of some molecules of synthetic or natural drugs such as cimetidine, azomycin and metronidazole. They have also exhibited important analytical properties in fluorescence and chemiluminescence [9-11]. Imidazole ring systems demonstrate various biochemical processes [12-14] and play a most important role in pharmaceutical activity. Imidazoles have been used in recent years as colouring supersensitized solar cells (DSSCs) [15,16], non-linear optics (NLO) [17,18] and organic light-emitting diodes (OLED) [19,20]. Substituted imidazole derivatives were revealed to exhibit remarkable fluorescent behaviour using simple, cost-effective applications of fluorescent sensors that were successfully used to achieve [21,22]. In addition, a unique solvatochromic behaviour of imidazole derivatives has been further explored, which can help in understanding the biological microenvironment [23-25]. In this work, we synthesized 4-(2-(4,5-dimethyl-2-(3,4,5-trimethoxyphenyl)-1*H*-imidazol-1-yl)ethyl)morpholine (DMTPM) and characterized with ^{1}H & ^{13}C NMR, HR-MS and single-crystal X-ray diffraction techniques. In addition, the DFT analysis such as molecular geometry parameter, Mulliken, MEP, NBO, HOMO-LUMO and thermodynamic properties were calculated using B3LYP/6-31G(d,p).

EXPERIMENTAL

Synthesis of 4-(2-(4,5-dimethyl-2-(3,4,5-trimethoxyphenyl)-1*H*-imidazol-1-yl)ethyl)morpholine (DMTPM): A mixture of butane-2,3-dione (1 mmol), 3,4,5-trimethoxybenzaldehyde (1 mmol), 2-morpholinoethanamine (1 mmol) and $C_2H_7NO_2$ (2 mmol) in the presence of SO_4^{2-}/Y_2O_3 catalyst (50

mg) in ethanol (20 mL) was refluxed [26]. The reaction blend was then stirred for 10 h at 80 ºC. The progress reaction was monitored *via* TLC. The crude yield was thus obtained by purifying the column chromatography with silica gel (100-120 mesh size) using hexane:ethyl acetate in the 4:1 (v/v) ratio as an eluent to the yield of tetrasubstituted imidazole (DMTPM). Yield 97%; white crystal; m.p. 90-93 ºC; ^{1}H NMR ($CDCl_3$, 400 MHz) δ 2.12 (d, *J* = 1.2 Hz, 6H), 2.25 (s, 4H), 2.45 (t, *J* = 7.2 Hz, 2H), 3.49 (s, 4H), 3.78 (d, *J* = 1.2 Hz, 9H), 3.97 (t, *J* = 6.8 Hz, 2H), 6.70 (s, 1H); ^{13}C NMR ($CDCl_3$, 100 MHz) δ 8.9, 11.4, 42.0, 53.7, 55.9, 56.2, 56.5, 58.3, 60.8, 66.4, 106.4, 106.7, 123.5, 124.9, 131.8, 138.7, 145.2, 150.2, 174.7; HRMS (ESI): calculated for $C_{20}H_{30}N_3O_4$ $[M+H]^+$ 376.2236; found 376.2238.

The synthesized compound ^{1}H & ^{13}C NMR spectrum was analyzed on $CDCl_3$ using a 400 MHz NMR spectrometer from Bruker Avance. The ^{1}H & ^{13}C NMR have been referred to TMS as an internal standard. A Bruker Maxis computer uses high-resolution mass spectra (HRMS) for electrospray ionization. Single crystal X-ray analysis for crystal was conducted in methanol. Diffraction results were collected at 295 K with a crystal size of 0.20 × 0.20 × 0.25 mm using a Bruker, 2004 APEX2 diffractometer with graphite monochromated MoKα radiation (λ = 0.71073 Å). The structure was analyzed by direct methods and refined by full-matrix least-squares calculations with the SHELXL program [27] with anisotropic thermal parameters. All non-hydrogen atoms and all the solvent atoms were refined anisotropically [28]. In addition, CCDC-1033634 for DMTPM, crystallographic data has been deposited with the Cambridge Crystallographic Data Centre.

Computational method: The molecular geometry of DMTPM was designed with a hybrid functional B3LYP/6-31G(d,p) basis set using the DFT process. All calculations were performed with software package Gaussian 03W [29]. The bond parameters, optimized structure, calculations for NLO, NBO, HOMO-LUMO and MEP were analyzed at the same stage of theory and plotted using the Gauss view method.

RESULTS AND DISCUSSION

4-(2-(4,5-Dimethyl-2-(3,4,5-trimethoxyphenyl)-1*H*-imidazol-1-yl)ethyl)morpholine (DMTPM) was synthesized by condensing butane-2,3-dione, trimethoxybenzaldehyde, 2-morpholinoethanamine and ammonium acetate in the sulphated yttria-catalyst ratio 1:1/1:2 using a multi-component one-pot reaction. The synthesized compound based on spectroscopic techniques (^{1}H & ^{13}C NMR, FT-IR and HRMS) was thoroughly characterized.

The aromatic protons are confirmed by ^{1}H NMR spectrum of DMTPM by the signal detected at δ 6.70 ppm with a sharp singlet of the integral value of two protons. One triplet with allocated methylene carbon C6 appeared in the higher frequency region at δ 3.97 ppm. The carbon C7 of the additional methylene protons appeared as a triplet at δ 2.45 ppm. The methoxy protons turned up at 3.78 ppm with an integral value of nine protons. Furthermore, two sets of methylene protons at N8 are allocated to deshielded signal appearing as a singlet at δ 3.49 ppm and the two methyl protons show up as a doublet at δ 2.12 ppm.

In ^{13}C NMR spectrum, a signal at δ 174.7 ppm is clearly due to C=N signal. The aromatic carbon signals appear at 153.6-106.4 ppm. The observed signals are allocated to CH_2 carbons C6 & C7 at δ 42.0 and δ 58.3 ppm and methylene carbon (C10 & C12) signal observed at δ 66.4 ppm. The signal at δ 53.7 ppm corresponds to methylene carbons at C9 & C13. At δ 58.3 ppm and the methoxy carbons appear at δ 56.3 ppm and the signals at δ 8.9 and 11.4 ppm are due to the two methyl carbons in C4 and C5. The high-resolution mass spectrum of DMTPMs, the $[M+H]^+$ signal measured at *m/z* 376.2236, is excellent compliance with the value calculated *m/z* 376.2238.

X-ray crystal structure: The crystal data and structure refinement parameters are given in Table-1 for title compound. The ORTEP of DMTPM is shown in Fig. 1. The crystallographic data of X-rays show that the DMTPM crystallized with space group p-1 in the triclinic system. In general, the length of the bond imine (C=N) is the estimated shorter than the length of the bond amine (C-N). In DMTPM, the bond distances for imine C7=N1 and amine C7-N2 are also 1.323 (4) and 1.363 (4) Å, showing the cyclic imine formation between atoms C7 and N1. The ring bonds of the distances selected are C8-C9 1.353 (5) Å, C8-N1 1.371 (5) Å, C9-N2 1.392 (5) Å, C11-N3 1.444 (4) Å, C13-O4 1.410 (7) Å, C14-O4 1.389 (7) Å and C15-N3 1.464 (5) Å. The molecule of the selected dihedral angles are C14-O4-C13-C12 58.0 (6)º, C14-C15-N3-C12 -56.3 (5)º, C14-C15-N3-C11 -178.3 (4)º, C15- C14-O4-C13 -56.5 (6)º, C10-C11-N3-C15 -172.7 (3)º, C11-C10-N2-C9 81.5 (4)º and C11-C10-N2-C7 -101.0 (6) (4)º. The data showed that two C-8 and C-9 methyl groups are in the same plane as the imidazole ring network, while the C-7 trisubstituted phenyl ring and the N-2 ethyl morpholine deviate with planarity. The respective 34.47º (N1–C7–C4–C3) and –101.09º (C7–N2–C10–C11). Table-2 listed the specified bond lengths, bond angles and torsion angles. A chair conformation is adopted by the

TABLE-1
CRYSTAL DATA AND STRUCTURE REFINEMENT FOR DMTPM

Parameters	DMTPM
Empirical formula	$C_{22}H_{33}N_3O_6$
Formula weight	435.51
Temperature (K)	295
Wavelength (λ)	0.71073 Å
Crystal system, space group	Triclinic, P-1
Unit cell dimensions	a = 10.1649(9) Å α = 107.413(8)°
	b = 11.4456(10) Å β = 90.023(7)°
	c = 11.7215(11) Å γ = 111.910(8)°
Volume (V)	1197.52(19) Å^3
Z, Calculated density	2, 1.208 Mg/m^3
Absorption coefficient	0.094 mm^{-1}
F(000)	468
Crystal size	0.20 × 0.20 × 0.25 mm
Theta range for data collection	2.7 to 26.3°
Limiting indices	-12<=h<=12, -12<=k<=14, -12<=l<=14
Reflections collected / unique	8627 / 4898 [R(int) = 0.029]
Final R indices [I>2σ(I)]	R1 = 0.1089, wR2 = 0.3295
R indices (all data)	R1 = 0.1597, wR2 = 0.3875
CCDC	1033634

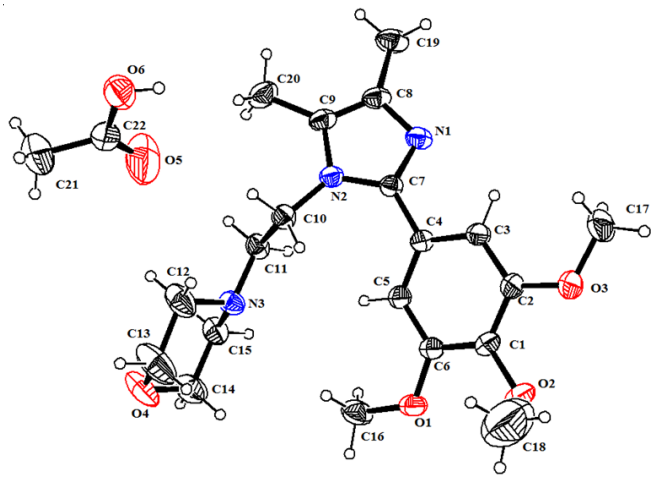

Fig. 1. ORTEP of 4-(2-(4,5-dimethyl-2-(3,4,5-tri-methoxyphenyl)-1*H*-imidazol-1-yl)ethyl)morpholine (DMTPM)

TABLE-2
SELECTED GEOMETRIC PARAMETERS BY X-RAY AND THEORETICAL CALCULATIONS FOR DMTPM AT B3LYP/6-311G (d, p) LEVEL

Bond lengths (Å)	XRD	B3LYP 6-31G(d, p)
C7-N1	1.323(4)	1.32430
C7-N2	1.363(4)	1.38324
C8-C9	1.353(5)	1.37994
C8-C19	1.488(5)	1.49759
C8-N1	1.371(5)	1.37233
C9-C20	1.496(6)	1.49394
C9-N2	1.392(5)	1.39276
C10-N2	1.459(4)	1.46337
C11-N3	1.444(4)	1.45396
C13-O4	1.410(7)	1.41889
C14-O4	1.389(7)	1.42768
C15-N3	1.464(5)	1.45691
Bond angles (°)		
N1-C7-N2	109.7(3)	111.00115
C9-C8-C19	128.6(4)	129.06682
C9-C8-N1	109.6(3)	110.23875
C19-C8-N1	121.8(3)	120.69300
C8-C9-C20	131.9(4)	131.09283
C8-C9-N2	105.9(3)	105.67511
C20-C9-N2	122.2(3)	123.20606
C11-C10-N2	111.3(3)	112.19305
C10-C11-N3	112.7(3)	118.17312
C13-C12-N3	109.3(4)	111.82580
C12-C13-O4	111.8(5)	110.37008
C15-C14-O4	112.3(4)	111.00762
C14-C15-N3	111.5(4)	113.09155
C7-N1-C8	107.4(3)	106.48723
C7-N2-C9	107.4(3)	106.59645
C7-N2-C10	128.1(3)	128.12842
C9-N2-C10	124.4(3)	124.91287
C11-N3-C12	113.3(3)	117.20120
C11-N3-C15	111.4(3)	118.00936
C12-N3-C15	108.5(3)	111.83951
C6-O1-C16	118.5(3)	120.29494
C1-O2-C18	115.8(6)	116.62336
C2-O3-C17	117.9(3)	118.06492
Torsional angles (°)		
N2-C7-N1-C8	-0.4(4)	0.17457
C4-C7-N2-C9	179.0(3)	-177.12591
C4-C7-N2-C10	1.2(6)	-3.84204
N1-C7-N2-C9	0.5(4)	0.05260
N1-C7-N2-C10	-177.4(3)	173.33646
C19-C8-C9-C20	-1.6(7)	2.66634
C19-C8-C9-N2	178.8(4)	-179.18715
N1-C8-C9-C20	179.8(4)	-177.77462
N1-C8-C9-N2	0.2(4)	0.37188
C9-C8-N1-C7	0.1(4)	-0.34290
C19-C8-N1-C7	-178.6(4)	179.25895
C8-C9-N2-C7	-0.4(4)	-0.25490
C8-C9-N2-C10	177.5(3)	-173.81346
C20-C9-N2-C7	179.9(4)	178.07565
C20-C9-N2-C10	-2.1(6)	4.51710
N2-C10-C11-N3	153.2(3)	-177.77925
C11-C10-N2-C7	-101.0(4)	103.38248
C11-C10-N2-C9	81.5(4)	-84.47312
C10-C11-N3-C12	64.6(4)	-65.17055
C10-C11-N3-C15	-172.7(3)	73.17261
N3-C12-C13-O4	-59.3(6)	-28.91218
C13-C12-N3-C11	-179.1(4)	109.36734
C13-C12-N3-C15	56.7(5)	-31.42091
C12-C13-O4-C14	58.0(6)	68.68825
O4-C14-C15-N3	56.7(5)	-19.23313
C15-C14-O4-C13	-56.5(6)	-42.67902
C14-C15-N3-C11	178.3(4)	-83.61464
C14-C15-N3-C12	-56.3(5)	56.82667

morpholine ring (N3/O4/C12-C15) The parameters for puckering are Q = 0.5596 (4) Å, = 176.74 (4)° and φ = 294.32 (5)° [30]. The crystal packing structure of DMTPM is shown in Fig. 2.

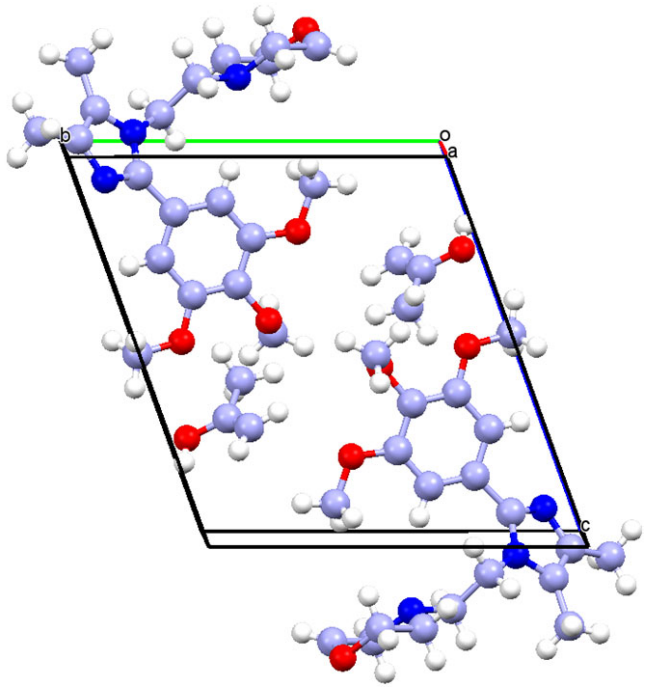

Fig. 2. Packing diagram of 4-(2-(4,5-dimethyl-2-(3,4,5-tri-methoxyphenyl)-1*H*-imidazol-1-yl)ethyl)morpholine (DMTPM)

Geometric analysis: The structural parameters of the synthesized DMTPM obtained from DFT/B3LYP/6-31G(d,p) were compared with single-crystal XRD. All the parameters agreed well with the XRD values. Table-2 provides the specified structural parameters. The optimized DMTPM structure is shown in Fig. 3.

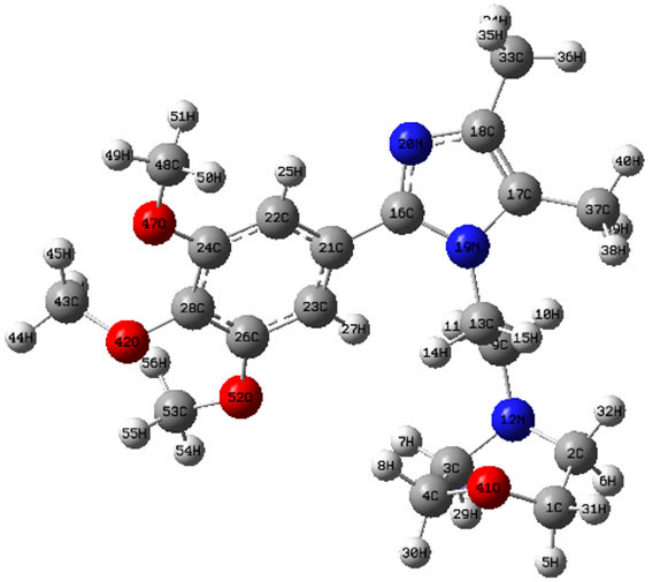

Fig. 3. Optimized structure of 4-(2-(4,5-dimethyl-2-(3,4,5-tri-methoxyphenyl)-1*H*-imidazol-1-yl)ethyl)morpholine (DMTPM)

HOMO-LUMO energies: Frontier molecular orbitals such as HOMO and LUMO were used to identify the molecular interactions in organic compounds. The FMO distance assists in characterizing the molecule's chemical reactivity and kinetic stability. A small orbital frontier distance with a molecule is more polarizable and more generally associated with greater chemical reactivity, lower kinetic stability and is often called a soft molecule [30]. The 3D FMO plots are shown in Fig. 4. The HOMO is found in the imidazole, morpholine and the phenyl rings at the imidazole and phenyl ring in the DMTPM, in the C-7 region. The energy gap obtained for title molecule was 3.2924 eV. DMTPM will be a better choice for electronic applications than the load-transfer relationship that ends.

NBO analysis: For DMTPM, natural bond orbital was performed at the DFT/B3LYP/6-31G(d,p) stage to elucidate intra-molecular, hybridization and delocalization within the molecule's electron density. The value of hyperconjugative EDT (interaction and transition of electron density) to lone

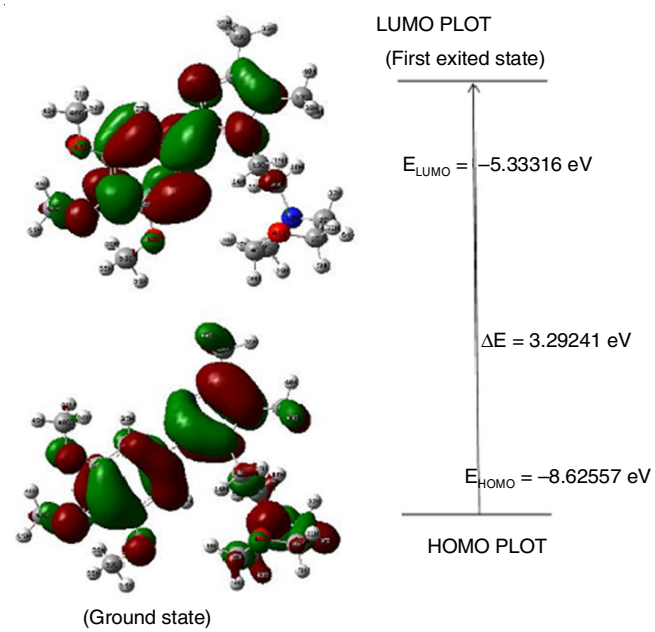

Fig. 4. HOMO and LUMO structure of 4-(2-(4,5-dimethyl-2-(3,4,5-tri-methoxyphenyl)-1*H*-imidazol-1-yl)ethyl)morpholine (DMTPM)

pair electrons was analyzed and the findings are summarized in Table-3. Several donor-acceptor interactions for imidazole were observed and among the most highest occupied. NBOs are the most critical delocalization sites in the network and the O and N atoms in the lone pairs (n). The intramolecular interaction is formed by the bonding (LPN19) and n(LPO47) and antibonding between π*(C16-N20) & π*(C17-C18) and π*(C22-C24) orbitals between the orbital overlap. Such interactions are observed in the C16-N20, C17-C18 and C22-C24 antibonding orbital with an increase in electron density that weakens the bonds. The most important interaction energies of n(LPN19) π-π*(C16-N20) & π*(C17-C18) and n(LPO47) π-π*(C22-C24) are 48.85, 31.37 and 29.11 kcal/mol, respectively. The greater energy helps the molecular structure with the stabilization.

Mulliken atomic charges: The Mulliken atomic charge of the DMTPM was calculated using the B3LYP/6-31G(d,p) level. This calculation depicts the charges in every atom of the molecule. The charge distribution structure is shown in Fig. 5. The O52 is considered more basic site than other atoms (52O = -0.544821a.u). The charge distribution of nitrogen and oxygen atoms present in the morpholine ring is also more basic (41O = -0.481659 a.u & 20N = -0.537469 a.u) 16C is considered more positive charge compared to other atoms (16C =

TABLE-3
SIGNIFICANT DONOR-ACCEPTOR INTERACTIONS OF DMTPM AND THEIR SECOND-ORDER PERTURBATION ENERGIES

Type	Donor (i)	ED/e	Acceptor (j)	ED/e	E(2) (kcal/mol)	E(j) – E(i) (a.u.)	F(i, j) (a.u.)
π-π*	C16-N20	1.83878	C17-C18	0.33196	21.97	0.34	0.080
π-π*	C21-C23	1.70001	C26-C28	0.41241	22.33	0.27	0.072
π-π*	C22-C24	1.69739	C21-C23	0.39465	20.45	0.30	0.071
π-π*	C26-C28	1.68493	C22-C24	0.38003	20.85	0.30	0.071
n-π*	LP(1) N19	1.56277	C16-N20	0.42433	48.85	0.28	0.104
n-π*	–	–	C17-C18	0.33196	31.37	0.30	0.089
n- π*	LP(2) O47	1.84606	C22-C24	0.38003	29.11	0.35	0.095

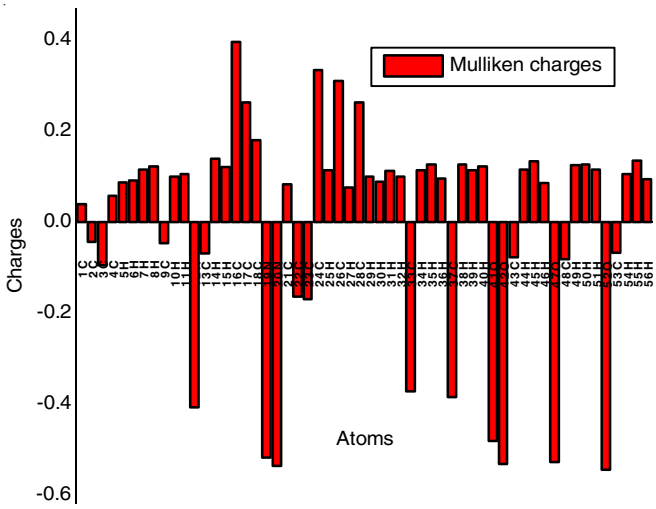

Fig. 5. Mulliken atomic charges of 4-(2-(4,5-dimethyl-2-(3,4,5-trimethoxyphenyl)-1*H*-imidazol-1-yl)ethyl)morpholine (DMTPM)

0.396183 a.u). The distribution of the charges indicates that the more negative the charges are concentrated on the oxygen and nitrogen atoms, the more positive charges are found in the hydrogens [31,32].

NLO effects: Non-linear optical is a forerunner of current research that provides key functions of optical switching, optical modulation, optical logic frequency shifting and optical memory in emerging technologies such as optical interconnections signal processing and telecommunications [33,34]. When describing non-linear optical properties, an external radiation field is often approximated as an external dipole moment. This external dipole moment is caused by a polarization molecule which is due to induced dipole moment. This molecular system of first hyperpolarizability (β_0) is calculated using the B3LYP/6-31G-(d,p) method, based on a finite field approach. The estimated DMTPM values for hyperpolarizability are given in Table-4. Urea is one of the reference molecules used in molecular systems to test NLO properties and also used for comparative purposes. The DMTPM measured first hyperpolarizability (β_{tot}) is 6.7777 $\times 10^{-30}$ esu, which is eighteen times greater than that of urea (β_{tot} 0.3728 $\times 10^{-30}$esu). Thus, this molecule may serve as a nonlinear optical material for a prospective building block.

Molecular electrostatic potential map: The MEP surface diagram is used to define a molecule as reactive behaviour, where negative regions with positive electrophilic sites can be considered nucleophilic centers and neutral regions. The MEP map of DMTPM (Fig. 6) suggests that the methoxy group and the N12, N19 and N20 atoms represent the most negative potential region but the N (nitrogen) atoms seem to be comparable to the small negative potential of the O (oxygen) atom. The H atoms attached to the six-membered rings bear the maximum charge of the (blue region) positive charge. The two extremes (dark blue and red colour) between a potential halfway to the MEP surface correspondence in the green region of the predominance.

Thermodynamic properties: On the source of vibrational investigation, the statistical thermodynamic functions *viz.*, the heat S^0_m (entropy), C^0_p (capacity), m and ΔH^0_m (enthalpy)

TABLE-4
MOLECULAR ELECTRIC DIPOLE MOMENT (μ) (Debye), POLARIZABILITY (α_0) AND HYPERPOLARIZABILITY (β_0) VALUES OF DMTPM

Parameters	B3LYP/6-31G(d,p)
Dipole moment (?) Debye	
μ_x	0.2882269
μ_y	-0.4412811
μ_z	-0.2231086
μ	0.57234 Debye
Polarizability (α_0) × 10^{-30} esu	
α_{xx}	322.5383691
α_{xy}	23.3236146
α_{yy}	295.8015294
α_{xz}	-8.2585235
α_{yz}	11.3039826
α_{zz}	158.6072677
α_0	0.67120 × 10^{-30} esu
Hyperpolarizability (β_0) × 10^{-30} esu	
β_{xxx}	-260.4087215
β_{xxy}	-516.2294762
β_{xyy}	-345.9189170
β_{yyy}	20.3705511
β_{xxz}	-31.1109397
β_{xyz}	33.8066695
β_{yyz}	18.0488183
β_{xzz}	13.9999788
β_{yzz}	-15.6380871
β_{zzz}	-41.6368227
β_0	6.77771 × 10^{-30} esu

Standard value for urea (μ = 1.3732 Debye, β_0 = 0.3728 × 10^{-30} esu): esu-electrostatic unit

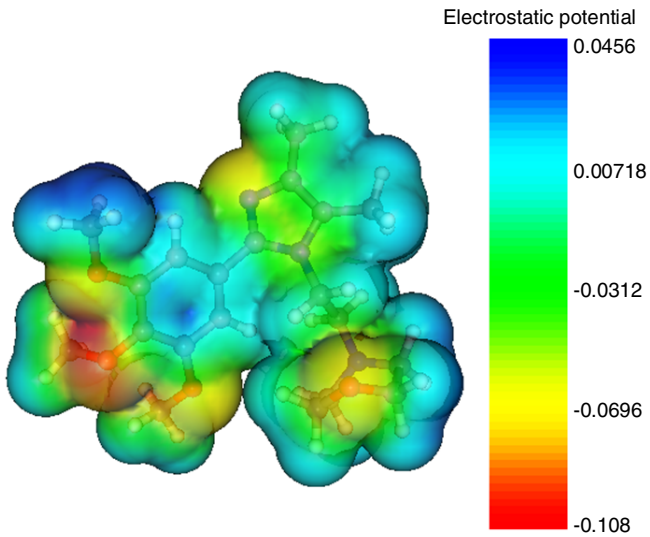

Fig. 6. MEP surface diagram of 4-(2-(4,5-dimethyl-2-(3,4,5-tri-methoxyphenyl)-1*H*-imidazol-1-yl)ethyl)morpholine (DMTPM)

changes of the DMTPM were obtained from theoretical harmonic frequencies. From Table-5, it can be fulfilled that these thermodynamic functions are those with rising temperature ranging from 100-1000 K with the fact that the molecular vibrational intensities increase with temperature. The thermodynamic properties of the correlation equations between heat

TABLE-5
THERMODYNAMIC PROPERTIES AT
DIFFERENT TEMPERATURE OF DMTPM

T (K)	S (J/mol K)	Cp (J/mol K)	ddH (kJ/mol)
100	463.55	203.92	12.25
200	643.25	324.71	38.86
300	797.26	444.73	77.25
400	942.22	568.14	127.93
500	1081.32	680.03	190.48
600	1213.94	774.83	263.36
700	1339.50	853.84	344.92
800	1457.96	919.94	433.70
900	1569.62	975.70	528.56
1000	1674.94	1023.06	628.56

entropy, capacity, enthalpy changes and temperatures were calculated by fitting the quadratic formulae and the corresponding fitting factors (R_2) to 0.999, 0.999 and 0.999, respectively. The DMTPM is shown for the temperature dependence of the heat capacity, entropy and enthalpy. The corresponding fitting equations are as follows:

$$C^0_{p,m} = 9.5422 + 0.04029 + 3.55927 \times 10^{-5}\ T^2\ (R^2 = 0.999)$$

$$S^0_m = 5.52418 + 0.02332 + 2.06054 \times 10^{-5}\ T^2\ (R^2 = 0.999)$$

$$\Delta H^0_m = 4.91692 + 0.02076 + 1.83403 \times 10^{-5}\ T^2\ (R^2 = 0.999)$$

Further studies on the thermodynamic data gives helpful information on the DMTPM. They can be used to calculate the further thermodynamic energies according to the thermodynamic functions of the relationships and to the chemical reactions of the thermodynamics second law.

Conclusion

In conclusion, a novel 4-(2-(4,5-dimethyl-2-(3,4,5-trimethoxyphenyl)-1*H*-imidazol-1-yl)ethyl)morpholine (DMTPM) was synthesized and their structure was confirmed ^{1}H & ^{13}C NMR, HR-MS and single-crystal X-ray diffraction. The X-ray data were compared with the DFT studies obtained from the data. All the theoretical bond parameters are in excellent conformity with the XRD values. Characterization of stabilization caused by ICT results from (LPN19) and π*(C16-N20) bond orbital overlap between the NBO results reflecting the charge transfer. The DMTPM of the molecular hyperpolarizability is 6.7777×10^{-30} esu and is about 18 times greater than the standard urea value (β of urea is 0.3728×10^{-30} esu). Hence, the DMTPM can be used as a potential NLO material. Thermodynamic functions such as heat capacity, entropy and enthalpy values increase with increasing temperature at a given temperature.

CONFLICT OF INTEREST

The authors declare that there is no conflict of interests regarding the publication of this article.

REFERENCES

1. K. Takagi, K. Kusafuka, Y. Ito, K. Yamauchi, K. Ito, R. Fukuda and M. Ehara, *J. Org. Chem.*, **80**, 7172 (2015); https://doi.org/10.1021/acs.joc.5b01028
2. W.-S. Huang, J.T. Lin, C.-H. Chien, Y.-T. Tao, S.-S. Sun and Y.-S. Wen, *Chem. Mater.*, **16**, 2480 (2004); https://doi.org/10.1021/cm0498943
3. C.H. Chen and J. Shi, *Coord. Chem. Rev.*, **171**, 161 (1998); https://doi.org/10.1016/S0010-8545(98)90027-3
4. T. Kamidate, T. Segawa, H. Watanabe and K. Yamaguchi, *Anal. Sci.*, **5**, 429 (1989); https://doi.org/10.2116/analsci.5.429
5. K. Nakashima, H. Yamasaki, N. Kuroda and S. Akiyama, *Anal. Chem.*, **51**, 2077 (1995); https://doi.org/10.1016/0003-2670(94)00360-X
6. A. MacDonald, K.W. Chain and T.A. Nieman, *Anal. Chem.*, **51**, 2077 (1979); https://doi.org/10.1021/ac50049a005
7. D.F. Marino and J.D. Ingle, *Anal. Chem.*, **53**, 294 (1981); https://doi.org/10.1021/ac00225a039
8. B.H. Lipshutz, *Chem. Rev.*, **86**, 795 (1986); https://doi.org/10.1021/cr00075a005
9. U. Ucucu, N.G. Karaburun and I.I.L. Isikdag, *Il Farmaco*, **56**, 285 (2001); https://doi.org/10.1016/S0014-827X(01)01076-X
10. K. Nakashima, Y. Taguchi, N. Kuroda, S. Akiyama and G. Duan, *J. Chromatogr.*, **619**, 1 (1993); https://doi.org/10.1016/0378-4347(93)80440-f
11. K. Yagi, C.F. Soong and M. Irie, *J. Org. Chem.*, **66**, 5419 (2001); https://doi.org/10.1021/jo010267w
12. J.G. Lombardino and E.H. Wiseman, *J. Med. Chem.*, **17**, 1182 (1974); https://doi.org/10.1021/jm00257a011
13. S. Balalaie and A. Arabanian, *Green Chem.*, **2**, 274 (2000); https://doi.org/10.1039/b006201o
14. S. Balalaie, M.M. Hashemi and M. Akhbari, *Tetrahedron Lett.*, **44**, 1709 (2003); https://doi.org/10.1016/S0040-4039(03)00018-2
15. M. Velusamy, Y.-C. Hsu, J.T. Lin, C.-W. Chang and C.-P. Hsu, *Chem. Asian J.*, **5**, 87 (2010); https://doi.org/10.1002/asia.200900244
16. D. Kumar, K.R.J. Thomas, C.-P. Lee and K.-C. Ho, *Org. Lett.*, **13**, 2622 (2011); https://doi.org/10.1021/ol2006874
17. E.M. Cross, K.M. White, R.S. Moshrefzadeh and C.V. Francis, *Macromolecules*, **28**, 2526 (1995); https://doi.org/10.1021/ma00111a055
18. J. Santos, E.A. Mintz, O. Zehnder, C. Bosshard, X.R. Bu and P. Gunter, *Tetrahedron Lett.*, **42**, 805 (2001); https://doi.org/10.1016/S0040-4039(00)02143-2
19. Z. Wang, P. Lu, S. Chen, Z. Gao, F. Shen, W. Zhang, Y. Xu, H.S. Kwok and Y. Ma, *J. Mater. Chem.*, **21**, 5451 (2011); https://doi.org/10.1039/c1jm10321k
20. X. Yang, S. Zheng, R. Bottger, H.S. Chae, T. Tanaka, S. Li, A. Mochizuki and G.E. Jabbour, *J. Phys. Chem. C*, **115**, 14347 (2011); https://doi.org/10.1021/jp203115c
21. M. Alfonso, A. Tárraga and P. Molina, *Org. Lett.*, **13**, 6432 (2011); https://doi.org/10.1021/ol202723d
22. M. Alfonso, A. Espinosa, A. Tárraga and P. Molina, *Org. Lett.*, **13**, 2078 (2011); https://doi.org/10.1021/ol2004935
23. S. Park, J.E. Kwon and S.Y. Park, *Phys. Chem. Chem. Phys.*, **14**, 8878 (2012); https://doi.org/10.1039/c2cp23894b
24. D. Kumar and K.R.J. Thomas, *J. Photochem. Photobiol. Chem.*, **218**, 162 (2011); https://doi.org/10.1016/j.jphotochem.2010.12.018
25. M. Szafran, A. Komasa and E. Bartoszak-Adamska, *J. Mol. Struct.*, **827**, 101 (2007); https://doi.org/10.1016/j.molstruc.2006.05.012
26. R. Rajkumar, A. Kamaraj and K. Krishnasamy, *J. Saudi Chem. Soc.*, **18**, 735 (2014); https://doi.org/10.1016/j.jscs.2014.08.001
27. G.M. Sheldrick, *Acta Crystallogr.*, **46**, 467 (1990); https://doi.org/10.1107/S0108767390000277
28. G.M. Sheldrick, SHELXL-97, Program for the Refinement of Crystal Structures, Germany (1997).
29. M.J. Frisch *et al.*, Gaussian 03 Revision E.01, Gaussian Inc Wallingford CT (2004).
30. S. Amala, G. Rajarajan, E. Dhineshkumar, V. Thanikachalam and M.A. Doss, *Asian J. Chem.*, **32**, 174 (2019); https://doi.org/10.14233/ajchem.2020.22385
31. M.A. Doss, G. Rajarajan, V. Thanikachalam, S. Selvanayagam and B. Sridhar, *J. Mol. Struct.*, **1158**, 277 (2018); https://doi.org/10.1016/j.molstruc.2018.01.012
32. S. Amala, G. Rajarajan, E. Dhineshkumar, M.A. Doss, V. Thanikachalam, S. Selvanayagam and B. Sridhar, *New J. Chem.*, **43**, 11003 (2019); https://doi.org/10.1039/C9NJ01631G
33. N. Acharjee and S. Mondal, *Asian J. Chem.*, **32**, 1191 (2020); https://doi.org/10.14233/ajchem.2020.22590
34. V. Arjunan, S. Senthilkumari and S. Mohan, *Asian J. Chem.*, **31**, 1737 (2019); https://doi.org/10.14233/ajchem.2019.22005